Nonlinear Dynamics in a Synthetic Momentum-State Lattice

Fangzhao Alex An,[1,*] Bhuvanesh Sundar[2,3,4] Junpeng Hou,[5] Xi-Wang Luo,[5] Eric J. Meier[1] Chuanwei Zhang,[5,†]
Kaden R. A. Hazzard[2,3,‡] and Bryce Gadway[1,§]

[1]*Department of Physics, University of Illinois at Urbana-Champaign, Urbana, Illinois 61801-3080, USA*
[2]*Department of Physics and Astronomy, Rice University, Houston, Texas 77005, USA*
[3]*Rice Center for Quantum Materials, Rice University, Houston, Texas 77005, USA*
[4]*JILA, Department of Physics, University of Colorado, Boulder, Colorado 80309, USA*
[5]*Department of Physics, The University of Texas at Dallas, Richardson, Texas 75080-3021, USA*

The scope of analog simulation in atomic, molecular, and optical systems has expanded greatly over the past decades. Recently, the idea of synthetic dimensions—in which transport occurs in a space spanned by internal or motional states coupled by field-driven transitions—has played a key role in this expansion. While approaches based on synthetic dimensions have led to rapid advances in single-particle Hamiltonian engineering, strong interaction effects have been conspicuously absent from most synthetic dimensions platforms. Here, in a lattice of coupled atomic momentum states, we show that atomic interactions result in large and qualitative changes to dynamics in the synthetic dimension. We explore how the interplay of nonlinear interactions and coherent tunneling enriches the dynamics of a one-band tight-binding model giving rise to macroscopic self-trapping and phase-driven Josephson dynamics with a nonsinusoidal current-phase relationship, which can be viewed as stemming from a nonlinear band structure arising from interactions.

The concept of synthetic dimensions [1], where motion in space is abstracted to encompass dynamics in spaces spanned by internal [2–6] or discrete motional states [7–9], has led to new capabilities for analog simulation with quantum matter [10–34]. Under this approach, the role of synthetic lattice sites is played by discrete internal or motional states, and tunneling between the sites is accomplished by driving state-to-state transitions. The spectroscopic control over the resulting tight-binding model, including direct control over tunneling phases, opens up new capabilities for Hamiltonian engineering. By combining these new possibilities for single-particle control with the native interactions in atomic and molecular systems [5,6,35–39], synthetic dimensions hold much promise for the exploration of exotic many-body physics.

To date, studies based on synthetic dimensions have almost uniformly been restricted to the noninteracting regime, or regimes in which there are mostly subtle modifications to the system's behavior [22,23,27,40]. Here, using lattices of atomic momentum states, we observe that the dynamics in the synthetic dimension is qualitatively altered by the presence of nonlinear atomic interactions. The controlled addition of atomic interactions to even a simple one-band tight-binding model leads to a rich variety of phenomena, including the transition to a macroscopically self-trapped regime and the appearance of a nonsinusoidal current-phase relationship in phase-driven Josephson dynamics, which we observe with single-site

resolution in the synthetic dimension. We note that these observations can be viewed as resulting from the emergence of a nonlinear band structure arising from interactions [41,42]. As synthetic lattices can readily incorporate designer disorder, gauge fields, and other features, these results pave the way for future explorations of novel collective phenomena in synthetic dimensions.

Figure 1 depicts our approach based on atomic momentum states [7,17]. A Bose-Einstein condensate (BEC) containing $\sim 10^5$ ^{87}Rb atoms is subjected to two counter-propagating lasers (wavelength $\lambda = 1064$ nm, wave vector $k = 2\pi/\lambda$) that both trap the atoms and couple the atomic momentum states. These laser fields allow for discrete momentum transfer to the atoms in units of two-photon recoil momenta $2\hbar k$ defining a set of states with momenta $p_n = 2n\hbar k$ and energies $E_n = p_n^2/2M$, with M the atomic mass. Because the energy difference between adjacent states p_n and p_{n+1} is unique, we individually address various nearest-neighbor transitions simply by driving the atoms with a comb of discrete frequency components. We write a controlled spectrum of frequency components onto one of the lasers, such that the interference between the multifrequency beam (colored arrows) and the single-frequency beam (black arrows) addresses two-photon Bragg transitions between many pairs of momentum states. This creates a lattice of states in a synthetic dimension (momentum), where all tunneling amplitudes, tunneling phases, and site energies are controlled by the amplitudes,
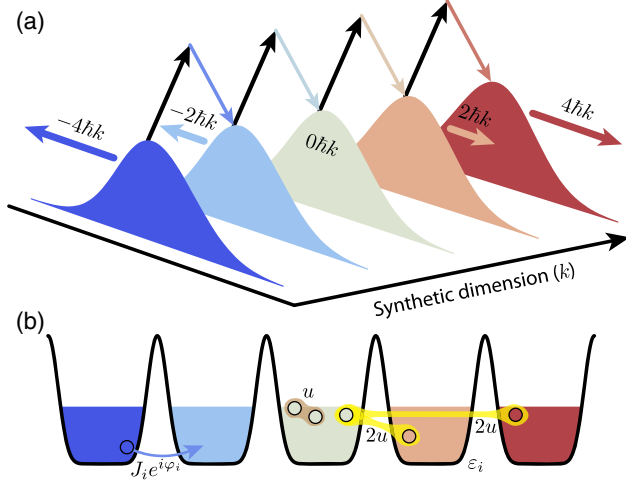
FIG. 1. Synthetic momentum-state lattices with atom-atom interactions. (a) Two-photon Bragg transitions individually couple atomic momentum modes along a synthetic dimension. (b) The synthetic lattice features intersite tunneling terms with controlled amplitude J_i and phase φ_i set by the Bragg laser amplitudes and phases, lattice site energies ε_i set by the two-photon Bragg detuning, and naturally occurring long-ranged and mode-dependent atomic interactions: Atoms in the same site experience a repulsive pairwise interaction of strength u, and atoms in different sites have a repulsive interaction of strength $2u$.

$$H = -J\sum_i(c_i^\dagger c_{i+1} + \text{H.c.}) - \frac{u}{2}\sum_i n_i^2. \qquad (1)$$

Here, i and j index the synthetic lattice sites, and $n_i = c_i^\dagger c_i$ is the number operator for site i, with c_i and $c_i^\dagger$ the site-i annihilation and creation operators, respectively.

We begin with all atoms in the nearly pure BEC and compose the Bragg frequencies such that the $k = 0$ mode relates to the central lattice site, as depicted in Fig. 2(a). We note that, because each synthetic site hosts only one discrete state, the lattice is intrinsically single band, with a simple cosine energy dispersion and a total bandwidth of $4J$. Initializing at a single site projects the atoms onto a superposition of all eigenstates in the band structure, giving rise to nonequilibrium dynamics and ballistic transport across the lattice [17,21], as shown in Fig. 2(b) in the limit where tunneling [$J/h = 1281(5)$ Hz] exceeds the collective interaction shift ($U/h = 520$ Hz).

We expect that, at weaker J, the nonlinear interactions can compete with the tunneling and influence the

phases, and detunings from Bragg resonance of the corresponding laser frequency components [17]. The site populations are all simultaneously measured via time-of-flight absorption imaging.

We briefly summarize how atomic collisions lead to relevant interactions in synthetic lattices of atomic momentum states [35,43]. The strength of the collisional interaction is $U = g\rho = (4\pi\hbar^2 a/M)\rho$, where a is the s-wave scattering length ($\sim$100 a_0 for ^{87}Rb), and ρ is the real-space atomic density. In momentum space, the s-wave collision is ostensibly all to all and state independent. However, quantum statistics leads to a natural state dependence to the interactions. A pair of atoms occupying the same momentum-state experience a direct interaction term $u = U/N$. In contrast, a pair of atoms occupying distinguishable momentum states experience an additional exchange energy due to bosonic exchange statistics, resulting in a total interaction of $2u$ [Fig. 1(b)].

In Ref. [35], we laid the groundwork for interactions in momentum-state lattices and their influence on a double-well system. Here, we explore the simplest one-dimensional lattice, with uniform nearest-neighbor tunneling J between 21 sites. Following the above discussion, the interaction is approximately [44] described by $u\sum_i n_i(n_i-1)/2 + 2u\sum_{i<j} n_i n_j = U(N - 1/2) - (u/2)\sum_i n_i^2$. This yields, up to irrelevant energy shifts, the combined Hamiltonian
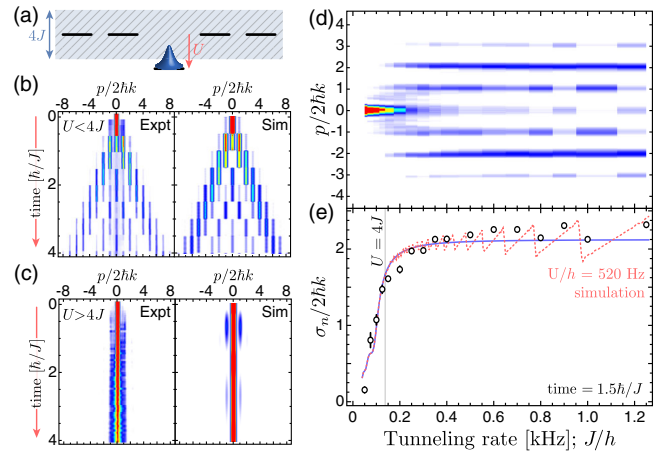

FIG. 2. Macroscopic self-trapping in an array of laser-coupled momentum states. (a) Atoms initialized to a single lattice site evolve in a one-dimensional lattice with uniform tunneling J. Self-trapping occurs when the collective interaction strength U exceeds the tunneling bandwidth $4J$. (b),(c) Population dynamics for strong [$J/h = 1281(5)$ Hz] and weak tunneling [$J/h = 93.3(2)$ Hz]. Left: data from integrated optical density (OD) images after 18 ms time of flight averaged over five experimental realizations. Right: dynamics from numerical simulations. (d) Integrated OD images plotted vs the tunneling strength J taken at times of $t = 1.5\hbar/J$. (e) Standard deviation of the atomic distributions from (d) shown alongside the simulation results. The solid blue curve assumes the ideal Hamiltonian after application of the rotating wave approximation, while the dashed red curve includes residual time dependence due to off-resonant effects. The expected self-trapping transition $U/J = 4$ is shown as a vertical gray line. Data for (d),(e) are averaged over 20 experimental realizations, and the error bars in (e) are the standard error of the mean. Numerical simulations in (b),(c),(e) assume a homogeneous mean-field energy of $U/h = 520$ Hz.

dynamics. In particular, when the nonlinear interaction strength U becomes greater than the full tunneling bandwidth $4J$, the atoms should be prevented from spreading in a solitonlike state. That is, tunneling from the initially occupied mode will be suppressed by being off resonant in energy with the other modes, a mechanism known as macroscopic quantum self-trapping [46,47]. Figure 2(c) shows such a lack of dynamics in the weak-tunneling regime [$J/h = 93.3(2)$ Hz], with atoms largely remaining on the initially populated site. Dynamics in both the strong- and weak-tunneling limits are in good agreement with Gross-Pitaevskii equation (GPE) simulations, which, for simplicity, approximate the trapped condensate as having a uniform mean-field energy of $U/h = 520$ Hz [44]. Figure 2(d) shows the transition from ballistic spreading to self-trapping more comprehensively for a range of tunneling rates. All data are taken at equivalent evolution times of $t = 1.5\hbar/J$. For large J, the ballistic evolution leads to a bimodal distribution peaked around the $\pm 4\hbar k$ states. As the tunneling rate decreases and interactions begin to dominate, the population is found to spread less far out, eventually remaining fully within the initialized site in the self-trapping region. By plotting the distribution width σ_n for each J in Fig. 2(e), we see that it is nearly constant at large J and that there is a rather steep turnover at low J values, in good agreement with the GPE simulations.

This direct site-resolved observation of macroscopic self-trapping, in excellent agreement with the Gross-Pitaevskii mean-field simulations [44], underscores the

coherent interplay between tunneling dynamics and atomic interactions in our synthetic lattice. We note that, while there have been numerous explorations of self-trapping [48–56] and other Josephson phenomena [57–64] in real-space potentials and in few-state spin mixtures [49,65–67], this is the first such observation in a many-site synthetic lattice. The incredible control over synthetic lattices promises the extension to future explorations of more complex dynamical phase transitions [68], including those of non-ground states [69].

We now move to make use of one of the most immediate and unique tools of synthetic lattices, the direct control of tunneling phase [36]. Specifically, we utilize this phase control to initialize superposition states with atoms delocalized over two adjacent sites and with a relative phase ϕ, as illustrated in Fig. 3(a). We then probe the phase-driven Josephson dynamics [46,70] in our many-site lattice by suddenly turning on the tunnelings and allowing the initialized wave packet to evolve for two tunneling times. As in the case of single-site initialization, there will be a propensity for the atoms to spread out across the lattice due to coherent tunneling. In addition, the relative phase ϕ can act to drive a net current of atoms in the lattice. In this case of phase-driven dynamics, we again expect interactions to play a nontrivial role.

We can gain some insight into the expected phase-dependent dynamics of our initial two-site wave packets by considering their far-field response, and by considering their distribution after two tunneling times as an
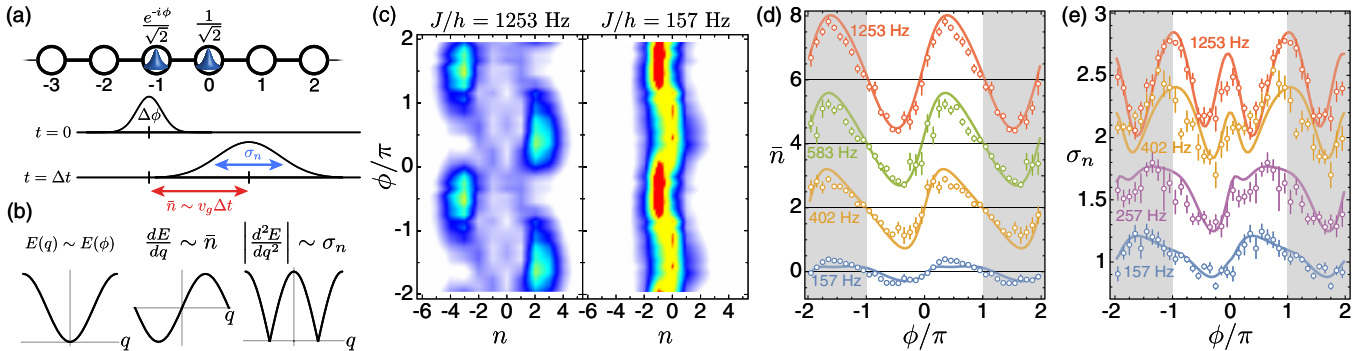

FIG. 3. Phase-driven dynamics in a synthetic bosonic Josephson junction array. (a) Atoms are prepared in a superposition state on two lattice sites $n = -1$ and $n = 0$ with equal weight and a relative phase of ϕ. Starting at time $t = 0$, the full lattice is turned on and the atoms evolve for a time Δt. We then measure the atomic distribution, from which we determine the mean displacement $\bar{n}$ (mean position $+0.5$) and spread σ_n (standard deviation of position) of the wave packet. (b) In the noninteracting limit, $\bar{n}$ and σ_n can be related to the single-band energy $E(q)$ of quasimomentum states in the synthetic lattice, as the wave packets with phase offset ϕ populate a spread of quasimomentum states about a mean synthetic quasimomentum $q_0 = \phi$. The plots show the band energy $E(q)$, the group velocity $v_g \propto dE/dq$, and the dispersion d^2E/dq^2 of the synthetic lattice. (c) Integrated density patterns (after two tunneling times) vs ϕ for the regimes of strong [left, $J/h = 1253(12)$ Hz] and weak tunneling [right, $J/h = 156.7(1.3)$ Hz]. (d),(e) $\bar{n}$ vs ϕ and σ_n vs ϕ, respectively, for several tunneling values [$J/h = \{156.7(1.3), 257(3), 402(3), 583(6), 1253(12)\}$]. Dots are experimental data and the lines are theory. The results for different tunneling values are offset for clarity in (d). No offset is applied for (e). The theory curves in (d),(e) are based on a real-space GPE simulation, as described in the text. Data for (c)–(e) are averaged over ten experimental realizations, with error bars in (d),(e) representing the standard error of the mean. The datasets in (c)–(e) were taken over a 2π range of ϕ values, uniformly shifted in phase to correct for phase shifts acquired during the wave packet initialization, and then mapped onto a larger and redundant 4π range. These redundant regions are distinguished by a gray background.

approximation thereof. We expect the average displacement $\bar{n}$ in the lattice after the quench time to be roughly proportional to the group velocity v_g of the initialized wave packet. Correspondingly, the spread (standard deviation) of the distribution after the quench σ_n should correspond to the spread in group velocities of the initialized wave packet. In the absence of interactions, the group velocity and dispersion (spread in group velocity) of our initialized two-site wave packets would be determined by the simple cosine band structure of the synthetic tight-binding lattice. That is, the initialization procedure will populate a range of Bloch-like states with an average synthetic quasimomentum of $q_0 = \phi$.

As shown in Fig. 3(a), the measured displacement and spread of the final distribution thus serve as probes of the synthetic band structure, at least in the noninteracting limit. Figure 3(b) provides an intuitive picture for the expected phase-driven dynamics in the $U = 0$ limit. The measured displacement $\bar{n}$ proportional to the group velocity v_g should scale as the first derivative of the band structure, i.e., with $\partial E / \partial q \propto \sin(\phi)$. More generally (away from $U = 0$), measurement of $\bar{n}$ vs ϕ probes the current-phase relationship (CPR) [71] of this synthetic bosonic Josephson junction array. Similarly, in the $U = 0$ and far-field limit, one expects the measured width σ_n to scale as the magnitude of the second derivative of the band structure, i.e., with $|\partial^2 E / \partial q^2| \propto |\cos(\phi)|$.

Figure 3(c) depicts the evolved atomic distributions in the tunneling-dominated regime [left, $J/h = 1253(12)$ Hz] and interaction-dominated regime [right, $J/h = 156.7(1.3)$ Hz], with plots of the integrated density patterns vs ϕ. In the large J limit, where interactions play a minor role, we indeed see agreement with the above description: Atomic currents are driven in the positive (negative) direction when the sinusoidal group velocity is maximally positive (negative) for ϕ values of $\pi/2$ ($-\pi/2$). At ϕ values of 0 and π, we find atoms flowing equally in the positive and negative direction, and the distribution has maximum width. As in Fig. 2, we again observe interference patterns of the atomic density in the inner region between right- and left-traveling wave fronts. In lowering J and entering into the interaction-dominated regime (right panel), we find dramatically different atomic distributions, with an almost complete collapse and absence of spreading, similar to the earlier self-trapped condition. However, we find that a clear ϕ dependence of the displacement survives, hinting at the formation of a partially mobile soliton.

A more quantitative analysis of the phase-driven dynamics is found in Figs. 3(d) and 3(e), with the ϕ dependence of $\bar{n}$ and σ_n shown for several J values. Even for the largest tunneling [$J/h = 1253(12)$ Hz], we observe a clear deviation from the $U = 0$ expectation. The measured CPR ($\bar{n}$ vs ϕ) deviates from the simple sine dependence, instead showing a skewed form that is in good agreement

with the numerical simulation curves, which are based upon real-space GPE simulations (solid line) [44]. Similarly, while in the noninteracting limit σ_n is π periodic with ϕ due to the insensitivity to the sign of the dispersion, we see that the distribution width is larger at the band edge ($\phi = \pm\pi$) than at the band center ($\phi = 0$).

While the density and scattering length of our atomic gas are fixed, we can increase the ratio U/J to explore how the phase-driven dynamics are impacted as interactions play a more dominant role, by simply lowering the tunneling J (maintaining an evolution time of $2\hbar/J$). For decreased values of J (increased U/J values), we observe that the measured current-phase response becomes further skewed and nonsinusoidal.

For a general tunnel junction, a nonsinusoidal CPR can arise for a host of reasons [71]. In real materials [71–75] and in real-space atomtronic junctions [76–82], such a skewed CPR can arise even in the absence of interactions between the current carriers, purely from the details of the junction. In our synthetic junction array, however, the "junctions" are featureless, simply relating to laser-driven state-to-state transitions. Still, even in this ideal synthetic junction array, it is predicted that nonlinear interactions alone can give rise to a skewed, nonsinusoidal CPR, as seen from the theory comparisons for increasing U/J [44]. In addition to becoming skewed, the overall amplitude of the CPR becomes suppressed as U/J increases. This muted response signals that the atoms of the fluid become effectively "heavier" as the collective interactions are increased relative to the tunneling. This can be interpreted in terms of a collapse of the effective nonlinear band structure as the atoms' effective mass increases and they behave like a collective soliton.

The dependence of the distribution widths σ_n on J can further shed light on how the atomic mobility is impacted by the increase in U/J [44]. We observe that the overall (ϕ-averaged) values of the σ_n are not so different for small U/J values [shown for the cases of $J/h = 402(3)$ Hz and 1253 (12) Hz]. For larger U/J values, we find that there is a marked collapse of the distribution widths, similar to that seen in Fig. 2(e). The dependence of σ_n on ϕ reveals additional features. The initial asymmetry in the σ_n values at $\phi = 0$ and $\pm\pi$ becomes more pronounced as the tunneling is decreased. Specifically, we find that the reduction in the measured σ_n for the central $\phi = 0$ feature occurs at larger J values (smaller U/J values) as compared to the broader $\phi = \pm\pi$ peaks. The GPE simulations show a similar response, with the central σ_n peak getting narrower and smaller before the decrease at $\phi = \pm\pi$. This signals a ϕ-dependent collapse of transport, with the atoms first becoming self-trapped for equal-phase superpositions ($\phi = 0$) and then, at larger U/J, for the out-of-phase state ($\phi = \pm\pi$). This behavior in our many-site array is reminiscent of the frequency response seen in Josephson double wells, where in-phase superposition modes are softened by

the introduction of nonlinear interactions, while the out-of-phase plasma mode acquires a stiffened response [46,51].

We note that the numerical simulation curves in Figs. 3(d) and 3(e) are based on real-space GPE calculations [44], which naturally incorporate the influence of the real-space trapping potential and the resulting inhomogeneous atomic density. This real-space treatment was necessitated by the use of a stiffer trapping potential characterized by a trapping frequency of 60 Hz along the spatial axis of the synthetic lattice (as compared to ∼10–15 Hz for the data of Fig. 2). This stiffer trap additionally led to a larger characteristic mean interaction strength, with a value of $\bar{U}/h = 1568$ Hz used in the simulation curves of Figs. 3(d) and 3(e). Importantly, the key observations of a nonsinusoidal CPR and a ϕ-dependent collapse of the distribution width are both found in ideal simulations that assume a homogeneous U term [44]. However, the real-space GPE analysis is key to capturing several finer features, or lack thereof, in the experimental data. Specifically, the effective spatial averaging over a range of U/J leads to an overall dulling of the ϕ-dependent collapse of σ_n. Similarly, GPE simulations with a uniform U predict an intriguing reversal of the atomic current (sign reversal of the CPR) over a range of U/J values close to the onset of self-trapping; however, this effect is not present in the real-space simulations. Finally, the drift of the data minima away from $\phi = 0$ in Fig. 3(e) seen for larger values of U/J stems from the real-space trapping potential and our exploring dynamics out to times that are not small compared to the trap period.

To conclude, we have performed the first measurements of significant interaction effects in a many-site synthetic lattice. These observations pave the way for the exploration of exotic nonlinear phenomena by straightforward extensions to more sophisticated synthetic lattices with gauge fields, disorder, and non-Hermiticity.

In addition to nonlinear phenomena captured by a classical mean-field description, atomic collisions [43] can also give rise to quantum correlations in synthetic momentum-state lattices, which can be explored through number-resolved imaging [83,84]. Furthermore, the extension of synthetic dimensions studies to spin systems [5,6,33] opens up a promising path to studying strongly correlated matter in synthetic dimensions.

[*]Present address: Honeywell Quantum Solutions, Golden Valley, Minnesota 55422, USA.
[†]chuanwei.zhang@utdallas.edu
[‡]kaden@rice.edu
[§]bgadway@illinois.edu

[1] T. Ozawa and H. M. Price, Nat. Rev. Phys. **1,** 349 (2019).
[2] O. Boada, A. Celi, J. I. Latorre, and M. Lewenstein, Phys. Rev. Lett. **108,** 133001 (2012).
[3] A. Celi, P. Massignan, J. Ruseckas, N. Goldman, I. B. Spielman, G. Juzeliūnas, and M. Lewenstein, Phys. Rev. Lett. **112,** 043001 (2014).
[4] M. L. Wall, A. P. Koller, S. Li, X. Zhang, N. R. Cooper, J. Ye, and A. M. Rey, Phys. Rev. Lett. **116,** 035301 (2016).
[5] B. Sundar, B. Gadway, and K. R. A. Hazzard, Sci. Rep. **8,** 3422 (2018).
[6] B. Sundar, M. Thibodeau, Z. Wang, B. Gadway, and K. R. A. Hazzard, Phys. Rev. A **99,** 013624 (2019).
[7] B. Gadway, Phys. Rev. A **92,** 043606 (2015).
[8] H. M. Price, T. Ozawa, and N. Goldman, Phys. Rev. A **95,** 023607 (2017).
[9] M. Heimsoth, D. Hochstuhl, C. E. Creffield, L. D. Carr, and F. Sols, New J. Phys. **15,** 103006 (2013).
[10] M. Mancini, G. Pagano, G. Cappellini, L. Livi, M. Rider, J. Catani, C. Sias, P. Zoller, M. Inguscio, M. Dalmonte, and L. Fallani, Science **349,** 1510 (2015).
[11] B. K. Stuhl, H.-I. Lu, L. M. Aycock, D. Genkina, and I. B. Spielman, Science **349,** 1514 (2015).
[12] L. F. Livi, G. Cappellini, M. Diem, L. Franchi, C. Clivati, M. Frittelli, F. Levi, D. Calonico, J. Catani, M. Inguscio, and L. Fallani, Phys. Rev. Lett. **117,** 220401 (2016).
[13] S. Kolkowitz, S. L. Bromley, T. Bothwell, M. L. Wall, G. E. Marti, A. P. Koller, X. Zhang, A. M. Rey, and J. Ye, Nature (London) **542,** 66 (2017).
[14] J. H. Kang, J. H. Han, and Y. Shin, Phys. Rev. Lett. **121,** 150403 (2018).
[15] J. H. Han, J. H. Kang, and Y. Shin, Phys. Rev. Lett. **122,** 065303 (2019).
[16] C.-H. Li, Y. Yan, S. Choudhury, D. B. Blasing, Q. Zhou, and Y. P. Chen, arXiv:1809.02122.
[17] E. J. Meier, F. A. An, and B. Gadway, Phys. Rev. A **93,** 051602(R) (2016).
[18] E. J. Meier, F. A. An, and B. Gadway, Nat. Commun. **7,** 13986 (2016).
[19] E. J. Meier, F. A. An, A. Dauphin, M. Maffei, P. Massignan, T. L. Hughes, and B. Gadway, Science **362,** 929 (2018).
[20] F. A. An, E. J. Meier, and B. Gadway, Sci. Adv. **3,** e1602685 (2017).
[21] F. A. An, E. J. Meier, and B. Gadway, Nat. Commun. **8,** 325 (2017).
[22] F. A. An, E. J. Meier, and B. Gadway, Phys. Rev. X **8,** 031045 (2018).
[23] F. A. An, K. Padavić, E. J. Meier, S. Hegde, S. Ganeshan, J. H. Pixley, S. Vishveshwara, and B. Gadway, Phys. Rev. Lett. **126,** 040603 (2021).
[24] S. Lapp, J. Ang'ong'a, F. A. An, and B. Gadway, New J. Phys. **21,** 045006 (2019).
[25] T. Xiao, D. Xie, W. Gou, T. Chen, T.-S. Deng, W. Yi, and B. Yan, Eur. Phys. J. D **74,** 152 (2020).
[26] W. Gou, T. Chen, D. Xie, T. Xiao, T.-S. Deng, B. Gadway, W. Yi, and B. Yan, Phys. Rev. Lett. **124,** 070402 (2020).

[27] D. Xie, T.-S. Deng, T. Xiao, W. Gou, T. Chen, W. Yi, and B. Yan, Phys. Rev. Lett. 124, 050502 (2020).

[28] D. Genkina, L. M. Aycock, H.-I. Lu, M. Lu, A. M. Pineiro, and I. B. Spielman, New J. Phys. 21, 053021 (2019).

[29] S. Sugawa, F. Salces-Carcoba, A. R. Perry, Y. Yue, and I. B. Spielman, Science 360, 1429 (2018).

[30] T. Chen, W. Gou, D. Xie, T. Xiao, W. Yi, J. Jing, and B. Yan, npj Quantum Inf. 7, 78 (2021).

[31] T. Xiao, D. Xie, Z. Dong, T. Chen, W. Yi, and B. Yan, arXiv:2011.03666.

[32] T. Chalopin, T. Satoor, A. Evrard, V. Makhalov, J. Dalibard, R. Lopes, and S. Nascimbene, Nat. Phys. 16, 1017 (2020).

[33] S. K. Kanungo, J. D. Whalen, Y. Lu, M. Yuan, S. Dasgupta, F. B. Dunning, K. R. A. Hazzard, and T. C. Killian, arXiv:2101.02871.

[34] J. A. Blackmore, P. D. Gregory, S. L. Bromley, and S. L. Cornish, Phys. Chem. Chem. Phys. 22, 27529 (2020).

[35] F. A. An, E. J. Meier, J. Ang'ong'a, and B. Gadway, Phys. Rev. Lett. 120, 040407 (2018).

[36] J. Hou, X.-W. Luo, K. Sun, T. Bersano, V. Gokhroo, S. Mossman, P. Engels, and C. Zhang, Phys. Rev. Lett. 120, 120401 (2018).

[37] S. Barbarino, L. Taddia, D. Rossini, L. Mazza, and R. Fazio, New J. Phys. 18, 035010 (2016).

[38] Q. Guan, T. M. Bersano, S. Mossman, P. Engels, and D. Blume, Phys. Rev. A 101, 063620 (2020).

[39] Q. Guan, M. K. H. Ome, T. M. Bersano, S. Mossman, P. Engels, and D. Blume, Phys. Rev. Lett. 125, 213401 (2020).

[40] S. L. Bromley, S. Kolkowitz, T. Bothwell, D. Kedar, A. Safavi-Naini, M. L. Wall, C. Salomon, A. M. Rey, and J. Ye, Nat. Phys. 14, 399 (2018).

[41] E. J. Mueller, Phys. Rev. A 66, 063603 (2002).

[42] S. B. Koller, E. A. Goldschmidt, R. C. Brown, R. Wyllie, R. M. Wilson, and J. V. Porto, Phys. Rev. A 94, 063634 (2016).

[43] R. Ozeri, N. Katz, J. Steinhauer, and N. Davidson, Rev. Mod. Phys. 77, 187 (2005).

[44] See Supplemental Material at http://link.aps.org/supplemental/10.1103/PhysRevLett.127.130401, which includes Ref. [45], for more experimental details and explanations of the different simulation techniques used in the Letter.

[45] P. Bader, S. Blanes, and F. Casas, J. Chem. Phys. 139, 124117 (2013).

[46] S. Raghavan, A. Smerzi, S. Fantoni, and S. R. Shenoy, Phys. Rev. A 59, 620 (1999).

[47] B. Juliá-Díaz, D. Dagnino, M. Lewenstein, J. Martorell, and A. Polls, Phys. Rev. A 81, 023615 (2010).

[48] M. Albiez, R. Gati, J. Fölling, S. Hunsmann, M. Cristiani, and M. K. Oberthaler, Phys. Rev. Lett. 95, 010402 (2005).

[49] T. Zibold, E. Nicklas, C. Gross, and M. K. Oberthaler, Phys. Rev. Lett. 105, 204101 (2010).

[50] Y.-A. Chen, S. D. Huber, S. Trotzky, I. Bloch, and E. Altman, Nat. Phys. 7, 61 (2011).

[51] G. Spagnolli, G. Semeghini, L. Masi, G. Ferioli, A. Trenkwalder, S. Coop, M. Landini, L. Pezzè, G. Modugno, M. Inguscio, A. Smerzi, and M. Fattori, Phys. Rev. Lett. 118, 230403 (2017).

[52] T. Anker, M. Albiez, R. Gati, S. Hunsmann, B. Eiermann, A. Trombettoni, and M. K. Oberthaler, Phys. Rev. Lett. 94, 020403 (2005).

[53] A. Reinhard, J.-F. Riou, L. A. Zundel, D. S. Weiss, S. Li, A. M. Rey, and R. Hipolito, Phys. Rev. Lett. 110, 033001 (2013).

[54] R. Labouvie, B. Santra, S. Heun, S. Wimberger, and H. Ott, Phys. Rev. Lett. 115, 050601 (2015).

[55] K. Xhani, L. Galantucci, C. F. Barenghi, G. Roati, A. Trombettoni, and N. P. Proukakis, New J. Phys. 22, 123006 (2020).

[56] S. Smale, P. He, B. A. Olsen, K. G. Jackson, H. Sharum, S. Trotzky, J. Marino, A. M. Rey, and J. H. Thywissen, Sci. Adv. 5, eaax1568 (2019).

[57] B. P. Anderson and M. A. Kasevich, Science 282, 1686 (1998).

[58] F. S. Cataliotti, S. Burger, C. Fort, P. Maddaloni, F. Minardi, A. Trombettoni, A. Smerzi, and M. Inguscio, Science 293, 843 (2001).

[59] S. Levy, E. Lahoud, I. Shomroni, and J. Steinhauer, Nature (London) 449, 579 (2007).

[60] L. J. LeBlanc, A. B. Bardon, J. McKeever, M. H. T. Extavour, D. Jervis, J. H. Thywissen, F. Piazza, and A. Smerzi, Phys. Rev. Lett. 106, 025302 (2011).

[61] M. Pigneur, T. Berrada, M. Bonneau, T. Schumm, E. Demler, and J. Schmiedmayer, Phys. Rev. Lett. 120, 173601 (2018).

[62] G. Valtolina, A. Burchianti, A. Amico, E. Neri, K. Xhani, J. A. Seman, A. Trombettoni, A. Smerzi, M. Zaccanti, M. Inguscio, and G. Roati, Science 350, 1505 (2015).

[63] V. Schweikhard, S. Tung, and E. A. Cornell, Phys. Rev. Lett. 99, 030401 (2007).

[64] S. Potnis, R. Ramos, K. Maeda, L. D. Carr, and A. M. Steinberg, Phys. Rev. Lett. 118, 060402 (2017).

[65] M.-S. Chang, Q. Qin, W. Zhang, L. You, and M. S. Chapman, Nat. Phys. 1, 111 (2005).

[66] A. Farolfi, A. Zenesini, D. Trypogeorgos, A. Recati, G. Lamporesi, and G. Ferrari, Phys. Rev. A 104, 023326 (2021).

[67] B. Evrard, A. Qu, K. Jiménez-García, J. Dalibard, and F. Gerbier, Phys. Rev. A 100, 023604 (2019).

[68] M. Heyl, Europhys. Lett. 125, 26001 (2019).

[69] T. Tian, H.-X. Yang, L.-Y. Qiu, H.-Y. Liang, Y.-B. Yang, Y. Xu, and L.-M. Duan, Phys. Rev. Lett. 124, 043001 (2020).

[70] B. Josephson, Phys. Lett. 1, 251 (1962).

[71] A. A. Golubov, M. Y. Kupriyanov, and E. Il'ichev, Rev. Mod. Phys. 76, 411 (2004).

[72] S. Hart, Z. Cui, G. Ménard, M. Deng, A. E. Antipov, R. M. Lutchyn, P. Krogstrup, C. M. Marcus, and K. A. Moler, Phys. Rev. B 100, 064523 (2019).

[73] J. J. A. Baselmans, A. F. Morpurgo, B. J. van Wees, and T. M. Klapwijk, Nature (London) 397, 43 (1999).

[74] J. A. van Dam, Y. V. Nazarov, E. P. A. M. Bakkers, S. De Franceschi, and L. P. Kouwenhoven, Nature (London) 442, 667 (2006).

[75] R. Delagrange, D. J. Luitz, R. Weil, A. Kasumov, V. Meden, H. Bouchiat, and R. Deblock, Phys. Rev. B 91, 241401(R) (2015).

[76] A. Ramanathan, K. C. Wright, S. R. Muniz, M. Zelan, W. T. Hill, C. J. Lobb, K. Helmerson, W. D. Phillips, and G. K. Campbell, Phys. Rev. Lett. **106**, 130401 (2011).

[77] S. Eckel, J. G. Lee, F. Jendrzejewski, N. Murray, C. W. Clark, C. J. Lobb, W. D. Phillips, M. Edwards, and G. K. Campbell, Nature (London) **506**, 200 (2014).

[78] S. Eckel, F. Jendrzejewski, A. Kumar, C. J. Lobb, and G. K. Campbell, Phys. Rev. X **4**, 031052 (2014).

[79] C. Ryu, P. W. Blackburn, A. A. Blinova, and M. G. Boshier, Phys. Rev. Lett. **111**, 205301 (2013).

[80] C.-C. Chien, S. Peotta, and M. Di Ventra, Nat. Phys. **11**, 998 (2015).

[81] G. Gauthier, S. S. Szigeti, M. T. Reeves, M. Baker, T. A. Bell, H. Rubinsztein-Dunlop, M. J. Davis, and T. W. Neely, Phys. Rev. Lett. **123**, 260402 (2019).

[82] C. Ryu, E. C. Samson, and M. G. Boshier, Nat. Commun. **11**, 3338 (2020).

[83] X.-Y. Luo, Y.-Q. Zou, L.-N. Wu, Q. Liu, M.-F. Han, M. K. Tey, and L. You, Science **355**, 620 (2017).

[84] A. Qu, B. Evrard, J. Dalibard, and F. Gerbier, Phys. Rev. Lett. **125**, 033401 (2020).